BNL-114206-2017-JA

Methanol Steam Reforming over Ni-CeO2 Model and Powder Catalysts: Pathways to High Stability and Selectivity for H2/CO2 Production

Z. Liu

Submitted to Catalysis Today

August 2017

Chemistry Department

Brookhaven National Laboratory

U.S. Department of Energy
USDOE Office of Science (SC),
Basic Energy Sciences (BES) (SC-22)

Notice: This manuscript has been authored by employees of Brookhaven Science Associates, LLC under Contract No. DE- SC0012704 with the U.S. Department of Energy. The publisher by accepting the manuscript for publication acknowledges that the United States Government retains a non-exclusive, paid-up, irrevocable, world-wide license to publish or reproduce the published form of this manuscript, or allow others to do so, for United States Government purposes.

DISCLAIMER

This report was prepared as an account of work sponsored by an agency of the United States Government. Neither the United States Government nor any agency thereof, nor any of their employees, nor any of their contractors, subcontractors, or their employees, makes any warranty, express or implied, or assumes any legal liability or responsibility for the accuracy, completeness, or any third party's use or the results of such use of any information, apparatus, product, or process disclosed, or represents that its use would not infringe privately owned rights. Reference herein to any specific commercial product, process, or service by trade name, trademark, manufacturer, or otherwise, does not necessarily constitute or imply its endorsement, recommendation, or favoring by the United States Government or any agency thereof or its contractors or subcontractors. The views and opinions of authors expressed herein do not necessarily state or reflect those of the United States Government or any agency thereof.

Methanol Steam Reforming over Ni-CeO_2 Model and Powder Catalysts: Pathways to High Stability and Selectivity for H_2/CO_2 Production

Zongyuan Liu [1], Siyu Yao [1], Aaron Johnston-Peck [2], Wenqian Xu [2], José A. Rodriguez [1 *], Sanjaya D. Senanayake [1 *]

[1] Chemistry Department,

[2] Center for Functional Nanomaterials

Brookhaven National Laboratory, Upton, NY, 11973

[*] Corresponding author: Bldg. 555A, Brookhaven National Lab,

P.O. Box 5000, Upton, NY 11973-5000,

Email: ssenanay@bnl.gov

Email: rodrigez@bnl.gov

Abstract

Nickel-ceria has been reported as a very good catalysts for the reforming of methane. Here, the methanol steam reforming reaction on both powder (Ni-CeO_2) and model (Ni-CeO_{2-x}(111)) catalysts was investigated. The active phase evolution and surface species transformation on powder catalysts were studied via *in situ* X-ray diffraction (XRD) and diffuse reflectance infrared transform spectroscopy (DRIFTS). Phase transitions of NiO → NiC → Ni and CeO_2 → CeO_{2-x} were observed during the reaction. The simultaneous production of H_2/CO_2 demonstrates that the active phase of the catalysts contains metallic Ni supported over partially reduced ceria. The DRIFTS experiments indicate that a methoxy to formate transition is associated with the reduction of ceria whereas the formation of carbonate species results from the presence of metallic Ni. A study of the reaction of methanol with Ni-CeO_{2-x}(111) by X-ray photoelectron spectroscopy (XPS) points to the essential role of metal-support interactions in an oxygen transfer from ceria to Ni that contributes to the high selectivity of the catalysts.

Keywords. Methanol steam reforming; nickel; ceria; in-situ XRD; ambient-pressure XPS; DRIFTS

1. Introduction

Although fuel cells are very attractive as an environmentally friendly technology, the application of a direct hydrogen fuel cell can be problematic due to the difficulties of transportation and storage of hydrogen. An alternative route is to make use of the so-called onboard fuel cell technology, where hydrogen is produced "onboard" to feed the cell through the steam reforming of alcohol [1, 2]. Owing to the absence of a C-C bond, steam reforming of methanol (MSR: $CH_3OH + H_2O \rightarrow CO_2 + 3H_2$) naturally has a lower activation temperature and better selectivity (less CO or coke formation) than other heavier alcohols [3]. This makes methanol as a promising candidate for onboard fuel cell applications.

Cu-based metal-oxides are the most common studied catalysts for methanol steam reforming because of copper's well-known capability of catalyzing methanol synthesis in the industry, which is a reverse way of the reforming reaction [4-8]. The main drawbacks of Cu-based catalysts used for MSR are their pyrophoricity and catalytic deactivation due to metal sintering. To overcome these issues, noble metals such as Pd [9-11], Pt [12, 13], and Au [14, 15] have been proposed for this reaction, and some of them exhibited catalytic activity comparable to that of Cu-based catalysts but with much better stability. Recently, Ni has been reported as a non-expensive alternative metal that shows promising catalytic activity and selectivity for the MSR reaction [16-18]. Although Ni on its own is vulnerable to the coke formation, in our earlier studies for methane and ethanol reforming, we have shown that a combination of Ni with ceria significantly inhibited the formation of surface carbon to steer the catalytic reaction to the desired pathways [19-22]. Furthermore, the superior ability of Ni-ceria to activate the C-H and/or O-H bonds in methane and ethanol indicates that this system could be a good catalyst for the MSR reaction as well.

Even though methanol is a simple C-1 molecule, the reaction mechanism for the MSR process remains split between two pathways including (1) a direct decomposition route and (2) a dehydrogenation route that involves a formate intermediate. Understanding better the reaction mechanism may point to a rational way of further improving the activity/selectivity of methanol steam reforming in fuel cell applications. Thus, numerous studies have been focused on revealing the catalytic active phase and identifying reaction intermediates, and some of these have provided interesting perspectives of the reaction pathways via *in situ* characterization techniques [12, 23-26]. In addition, adsorption and reaction of methanol on well-defined model surfaces have also been investigated extensively in the literature. Thus, articles have been reported studying the surface chemistry of this molecule on Cu(111) [27], Au(111) [28], Ni(111) [29, 30], Pt(111) [31, 32], CeO_2(111) [33, 34], TiO2(110) [35], Cu-TiO2(110) [36], and Pt-CeO_2(111) [37]. Nevertheless, none of the studies correlate the information from a perspective of both powder and model systems, and thus a molecular level understanding of the structure-reactivity relationship for methanol steam reforming is rather limited.

In this study, we deal with a Ni-CeO_2 catalyst that is active and selective for the methanol reforming reaction, and for the first time, powder and model system studies are combined to provide insights regarding structure-reactivity correlations, especially for the role of metal-oxide interactions in the catalytic selectivity. In this work, we first examined the performance of Ni-ceria catalyst for MSR by using *in situ* XRD and DRIFTS, aiming at elucidating the structure related surface mechanism under reaction conditions. Then, we correlated this knowledge with a study of the surface chemistry of methanol on a well-defined Ni-CeO_{2-x}(111) model system to further reveal the synergy between the metal and oxide support, and its effect on the catalytic selectivity to minimize CO production.

2. **Experimental**

Ni/CeO_2 was prepared by an incipient wetness impregnation method. 20% Nickel nitrate was mixed with cerium oxide in molar ratio. The sample was dried and calcined at 500 ˚C in air. Characterization by powder XRD showed that the as-prepared sample contained 8.5 wt % NiO and 91.5 wt % CeO_2, from which the calculated mole ratio of Ni to Ce is 0.21 to 1. The average crystal size estimated with XRD was 8 nm for CeO_2 and 12 nm for NiO. Following previous studies the content of nickel was kept small (< 10 wt %) to optimize catalyst performance [21,22].

Temperature-programmed reduction (TPR) and steam reforming experiments in conjunction with XRD and a residual gas analyzer (RGA) were performed at beamline X7B (λ=0.3196 Å) of the National Synchrotron Light Source (NSLS) at Brookhaven National Laboratory (BNL). Under room temperature, the saturation vapor pressure of methanol is 0.18 bar. The generation of the steam vapor ($MeOH/H_2O$ =1:3) was achieved by passing He through a bubbler filled with a mixture of methanol and water. The gas flow rate used in this study, 10 cc/min, was sufficiently low to guarantee that the gases passing through the bubbler reached a vapor saturated state. The reaction cell and other parts of the gas flow system have been described in detail elsewhere [38]. Powder samples of 2 - 3 mg were loaded into a silica capillary (0.9 mm ID, 1.0 mm OD) mounted in the flow cell system. A Perkin Elmer Amorphous Silicon Detector was used to collect two-dimensional transmission diffraction data, which were subsequently processed with the program Fit2D [39] to obtain XRD profiles (Intensity versus 2θ). Lattice parameters and phase quantities were analyzed by Rietveld Refinement using the program GSAS [40, 41].

DRIFTS data were collected on Ni/CeO_2 sample under steam reforming conditions using a Bruker Equinox 55 FTIR spectrometer equipped with a modified Harrick Praying Mantis DRIFTS cell connected to a gas flow system similar to the one used in XRD experiments. Details of the instrument can be found in ref [42]. The $MeOH/H_2O$ ratio was kept at 1/3.

Transmission electron microscopy (TEM) images were obtained using a JEOL JEM 2100 instrument operating with an acceleration voltage of 200 kV. Sample powders were dispersed as a suspension in deionized water and sonicated for 60s. After being well dispersed, a droplet of suspension was deposited on Holey-Carbon coated Cu grids and allowed to dry before imaging.

Soft X-ray photoelectron spectroscopy (XPS) was conducted using synchrotron radiation at beamline U12a at the National Synchrotron Light Source (NSLS). O 1s and C 1s sXPS were recorded using 700 and 395 eV photon energies for excitation, respectively. The instrumental resolution was ca. 0.2 eV. The Ce 4d photoemission lines were used for binding energy calibration using the 122.8 eV satellite features [43]. The methanol source (Pharmco-aaper, ACS/USP grade) was freeze-pumped-thawed in liquid nitrogen to remove gaseous contaminants. The adsorbate was introduced to the UHV chamber using a "backfilling" method via a high precision leak valve.

For $Ni\text{-}CeO_{2-x}(111)$ film preparation, Ce metal was first evaporated onto the Ru crystal held at 427 ^{o}C (700 K) in the presence of 5×10^{-7} Torr O_2, and then annealed at 527 ^{o}C (800 K) for 10 mins with the same O_2 pressure. For sub-stoichiometric film $CeO_{2-x}(111)$, 2×10^{-8} Torr O_2 pressure was used during the Ce deposition at 427 ^{o}C (700 K) [44], and a reduced surface containing ~40% Ce^{3+} was obtained, as determined by XPS. After deposition, the surface was subsequently annealed at 527 ^{o}C (800 K) in UHV for 10 mins. The ceria films were estimated to be ca. 2-4nm thick (7-10 layers of O-Ce-O) based on the attenuation of the Ru 3d XPS signal,

which can eliminate the interference of Ru $3d_{3/2}$ (284 eV) with the C 1s signal. Ni was vapor deposited on the as-prepared ceria film at 27 ^{o}C (300 K) under vacuum and then annealed at 427 ^{o}C (700 K) for 1min. Ni coverage was estimated by thermal desorption of CO/Ni-CeO_{2-x} [20], whereas desorption peak area was calibrated by the 0.58 monolayer (ML) saturation coverage of CO on clean Ru(0001) [45]. The deposition rate of Ni was estimated to be 0.20 ML/min.

3. Results and discussion

3.1. MSR over Powder Ni-CeO_2 Catalysts: Structure, Chemical State and Mechanism

Figure 1a shows a series of *in situ* XRD profiles of a NiO/CeO_2 precursor under temperature programmed reduction of methanol. The as-prepared catalyst contains NiO particles impregnated on the ceria support, as indicated by the NiO diffraction peaks in Figure 1a. As the temperature is increased, a NiO→Ni phase transition and a slight shift of the ceria peak position are clearly seen. Rietveld refinement was used to quantitatively analyze these phenomena as a function of temperature as shown in Figure 1b. The NiO phase starts to be reduced from 250 °C and a hexagonal intermediate phase emerged and then further transforms into metallic fcc-Ni from 400 °C, as marked in the upper panel of Figure 1b. This intermediate phase is assigned to a Ni carbide phase, which will be ascertained later from the XPS study. Additionally, through Rietveld refinement, we can also extract the CeO_x lattice parameter (Figure 1b). This can be monitored as a function of heating, depicting a nonlinear lattice expansion of ceria, and the expansion rate involved a sharp rate of increase from 225 to 260 °C. The non-thermal increase of the lattice constant suggests the reduction of Ce(IV) to Ce(III) occurs since Ce(III) ion has larger atomic radii [19]. As a result, in the TPR process, the catalyst transforms from NiO/CeO_2 to Ni/CeO_{2-x} which means that a significant amount of metallic Ni centers and O vacancies / Ce(III) sites are generated.

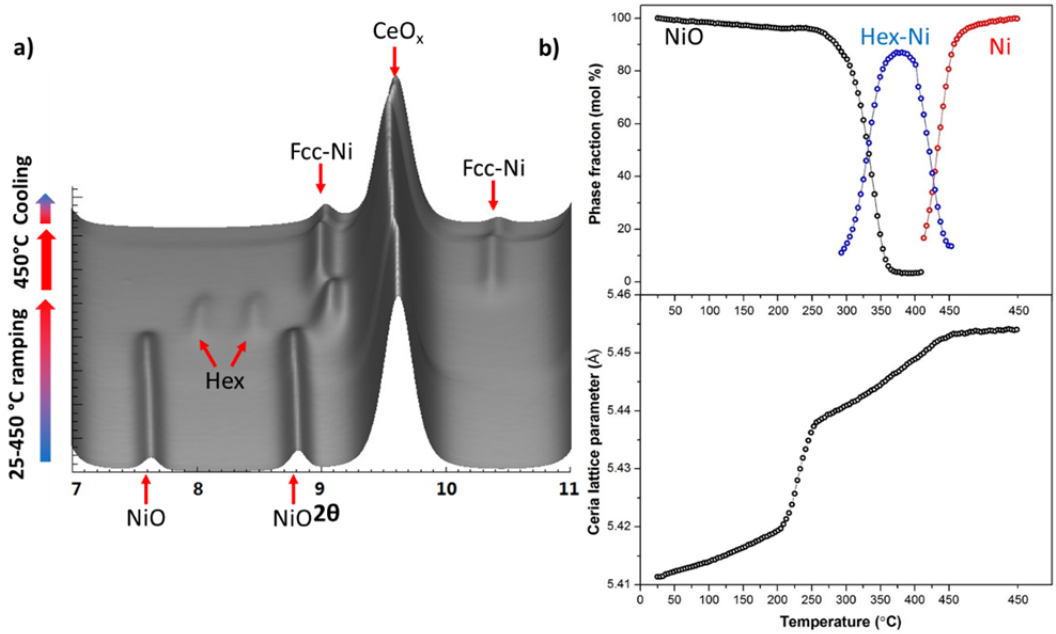

Figure 1 a): *In situ* XRD profiles of Ni/CeO_2 during the temperature-programmed reduction in pure MeOH vapor. b): Refinement: Phase evolution of NiO to metallic Ni (the upper panel) and the change of Lattice constant of CeO_2 (the lower panel)

The catalytic activity of the Ni-CeO_2 catalyst for methanol steam reforming was tested at a methanol/water ratio of 1/3. The sample was stepwise heated from 25-400 °C, meanwhile the phase evolution was recorded by the *in situ* XRD and the gas products were monitored by a mass spectrometer, as shown in Figure 2. Similar to the TPR reduction of methanol, Rietveld refinement of the phase transition plotted in the upper panel of Figure 2 indicates NiO was reduced to metallic Ni with the same nickel carbide intermediate phase appearing at temperatures around 250 °C. However, the amount of the Ni carbide phase formed in the methanol/water gas stream is much smaller than that under pure methanol vapor, suggesting that the presence of water inhibits the formation of Ni carbide. Moreover, as the temperature increased to 350 °C, the fast disappearance of Ni carbide associated with the sharp increase of metallic Ni indicates that water started precipitating into the reaction by taking C from Ni carbide, as evident by the CO/CO_2 production in the mass-spectrometer.

The catalytic activity associated with this chemical and structural transformations is shown in the lower panel of Figure 2. Before the reduction of NiO at 250 °C, the production of CO_2/H_2 was negligible. Once the NiO starts to be reduced after 250 °C, simultaneous production of CO_2/H_2 is seen. It should be noted that, initially from 250-300 °C, no metallic Ni but Ni carbide phase was formed, plus a small amount of CO was also produced. This implies that surface carbon formation may occur at this temperature range while methanol was reducing the NiO at the cost of generating Ni carbide/CO instead of CO_2, due to a poor oxidative environment. A further increase of the temperature up to 400 °C leads to the complete formation of metallic Ni, a steady-state was reached and the selectivity in favor of CO_2 over CO significantly increased at 400 °C. This result demonstrates that the active phase of the catalyst under steady reaction state contains metallic Ni supported over partially reduced ceria (Ce^{3+} rich). Moreover, it also indicates the participation of ceria in the re-oxidation of surface carbon as well as Ni carbide by providing lattice oxygen through the metal-oxide interfaces. The migration of O from ceria to Ni is an endothermic process with a thermodynamic barrier of 18 kcal/mol [46], suggesting this phenomenon needs higher temperature (>350 °C). The removal of surface carbon has also been confirmed by the post reaction TEM images (Figure 3). After reaction at 400 °C for 10 hours, the post reaction catalyst remains uniform with respect to particle size and no carbon fibers or graphite layers are seen.

Apart from the carbon-free reaction, CO_2 selectivity is also important for methanol steam reforming as the co-produced CO will poison the anode of fuel cells when H_2 is consumed [2]. Cu-based catalysts are the most commonly studied material for methanol steam reforming and increasing CO_2 selectivity while minimizing the CO formation is the target to attain [2, 3]. Thus, we have made a comparison of our Ni-CeO_2 to Cu-CeO_2 catalysts in terms of catalytic activity

and selectivity (Figure 4). Same amount of Cu to Ni loading with the similar preparation method was used for the comparison (20% in molar ratio to ceria). For methanol conversion, ceria oxide on its own is clearly not active. Pure NiO and Ni-CeO_2 catalysts exhibited very similar methanol activity while Cu-ceria catalyst started to activate methanol at 100 °C lower in comparison to the Ni catalysts. Eventually, the methanol conversion reached 100 % for the Cu and Ni catalysts at 400 °C. On the other hand, Cu-CeO_2 presented relatively high CO_2 selectivity in the temperature window of 200-300 °C but decayed as temperature increased to 400 °C. However, the Ni-CeO_2 catalyst shows much higher selectivity than either Cu-CeO_2 or NiO at temperature above 300 °C. The high conversion/selectivity of the Ni-CeO_2 catalyst at higher temperature can be attributed to the oxygen vacancies (Vac) created on the ceria surface that assist the water dissociation, and the strong metal-support interactions that facilitate the transferring of oxygen between ceria and Ni which will then aid the oxidation reactions. A complete reaction scheme will be shown at the end of the discussion.

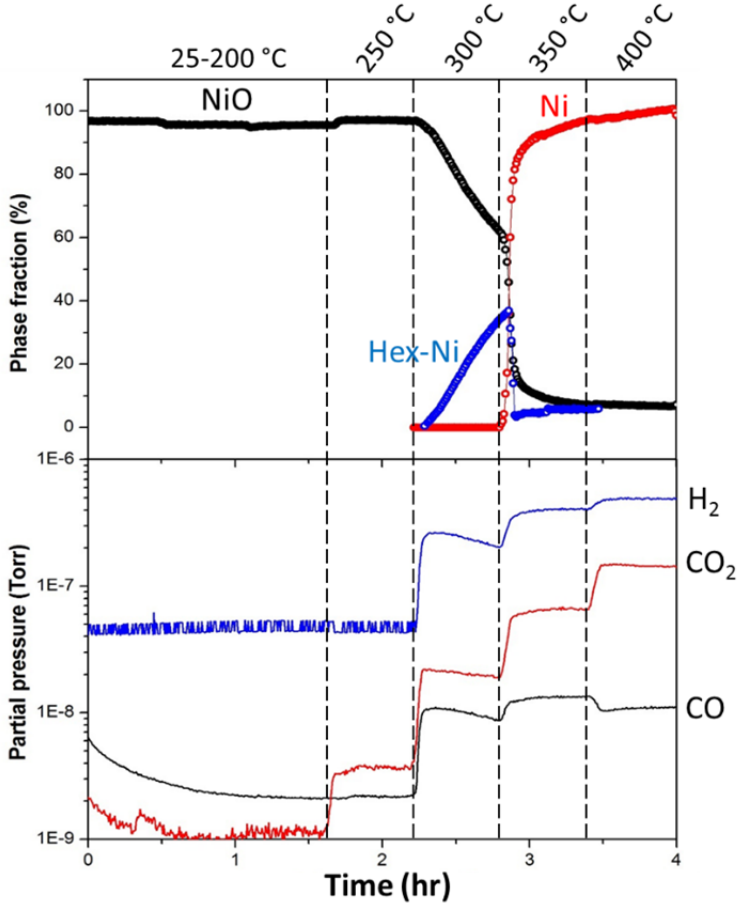

Figure 2 Phase evolution derived from *in situ* XRD (upper panel) and the products distribution derived from mass-spec data (the lower panel) during the steam reforming of methanol reaction.

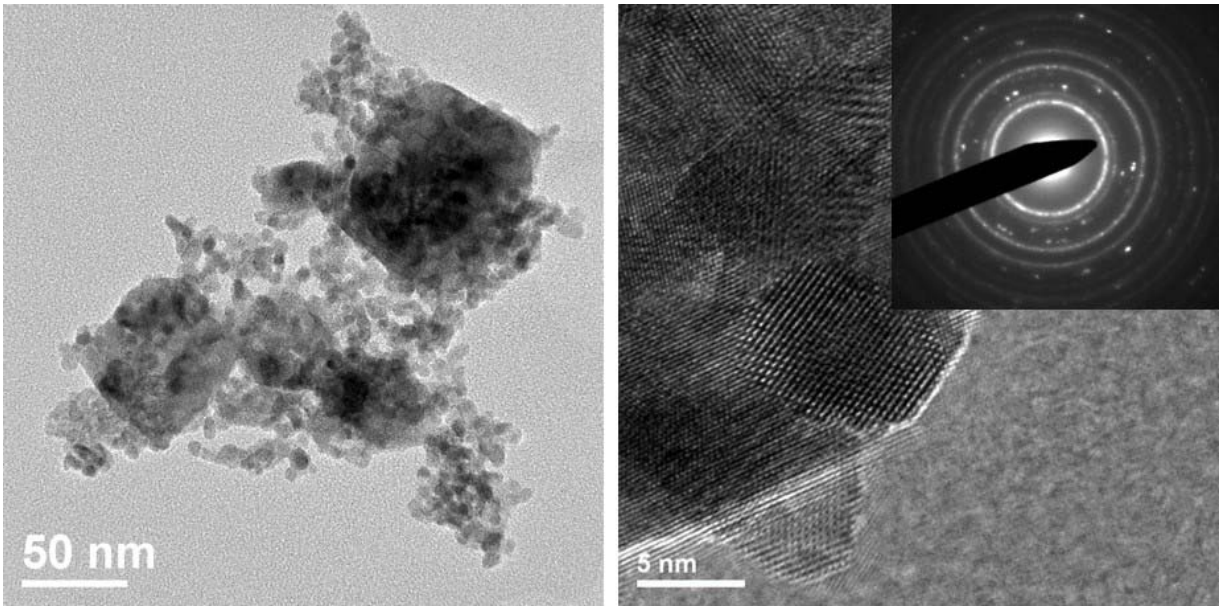

Figure 3 TEM images of the post-reaction Ni-CeO_2 sample, the inset figure displays the electron diffraction of the probing area. Metallic Ni was re-oxidized to NiO after the sample was exposed to air during the transfer to TEM imaging.

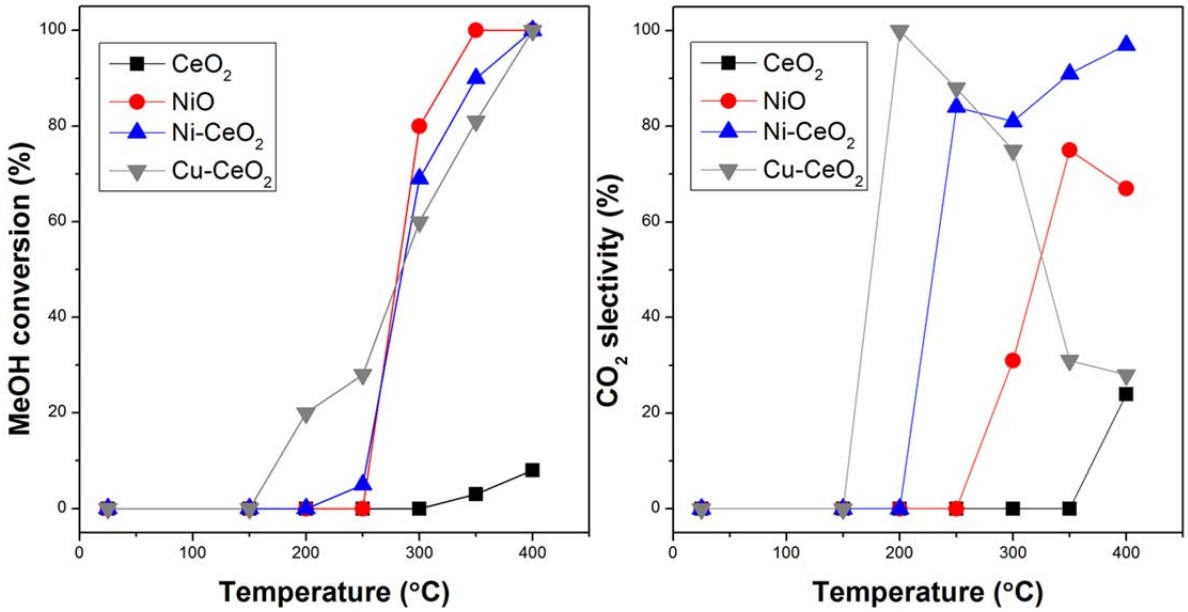

Figure 4 Methanol conversion and CO_2 selectivity towards CO as a function of temperatures over ceria, NiO, Ni-CeO_2 and Cu-CeO_2 catalysts.

To better understand the surface species associated with the reaction mechanism, we conducted *in situ* DRIFTS experiments for Ni-CeO_2 under MSR in similar condition as the XRD experiment, as shown in Figure 5. At room temperature, a broad bump from 3000 to 3600 cm^{-1} along with an OH scissoring band at 1650 cm^{-1} were identified for surface condensed water. Other features are also observed but difficult to identify due to the overlap with the water features. Increasing the temperature to 100 °C leads to the desorption of surface molecular water and reveals clear bands characteristic for methoxy (CH_3O-) species: 1103 cm^{-1} and 1048 cm^{-1} for the ν(CO) vibrational modes of methoxy in monodentate and bidentate configurations, respectively [12, 34]. The C-H stretching region from 2800-3000 cm^{-1} for methoxy is rather less well -defined, being rather broad and weak, but a sharp peak at 2800 cm^{-1} as indicative of symmetric methyl stretches ($\nu_s(CH_3)$) is detected [34]. The methoxy features then gradually diminish as the temperature is increased, while a series of new peaks appear, indicating the conversion of methoxy to other surface species. At 200 °C, peaks at 2840, 1555 and 1342 cm^{-1} are ascribed to formate (HCOO-) species for ν(CH), ν_{as}(OCO) and ν_s(OCO) vibrational modes, respectively, suggesting the transformation from methoxy to formate on the surface [12, 47, 48]. The band at 1427 cm^{-1} (ν(CO)) along with the peak at 852 cm^{-1} (π(CO)) may correspond to polydentate carbonate (CO_3) species [49, 50]. Upon further increase of the temperature up to 400 °C, a second transformation is observed, evident by the complete disappearance of the C-H stretching bands at 2800-3000 cm^{-1} as well as the ν(OCO) features for formate. In the meantime, two broad peaks centered at 1458 and 1377 cm^{-1} emerged accompanied by a small peak at 860 cm^{-1} at 400 °C. These two broad bands are most likely contributed from the overlap of various carbonate species with different adsorption modes, but the peak at 860 cm^{-1} could be unequivocally assigned to out-of-plane bending vibrations of carbonate species [47, 51].

Additionally, water dissociation is evident by the OH stretching band at 3620 cm^{-1} at 350 °C and it is rapidly consumed at 400 °C. Moreover, significant amounts of CO_2 production was detected above 350 °C with its gas phase centered at 2350 cm^{-1}. These results indicate that surface formate species are further oxidized to carbonate with the assist of hydroxyl groups from water, while the surface carbonates subsequently transformed to gas phase CO_2.

The evolution of surface species as seen in the *in situ* DRIFTS spectra could be correlated with the phase evolution discussed in Figure 1 and 2, where ceria gets reduced at 250 °C and metallic Ni appears from 350 °C. Thus, it is reasonable to validate that the methoxy to formate transition is associated with the reduction of ceria whereas the presence of metallic Ni above 350 °C results in the formation of carbonates by the decomposition of formates. Therefore, with a combination of *in situ* XRD and DRIFTS, we can conclude that the reaction pathway of Ni-CeO_2 catalyst favors the dehydrogenation route through several surface species including methoxy, formates, hydroxyls and carbonates.

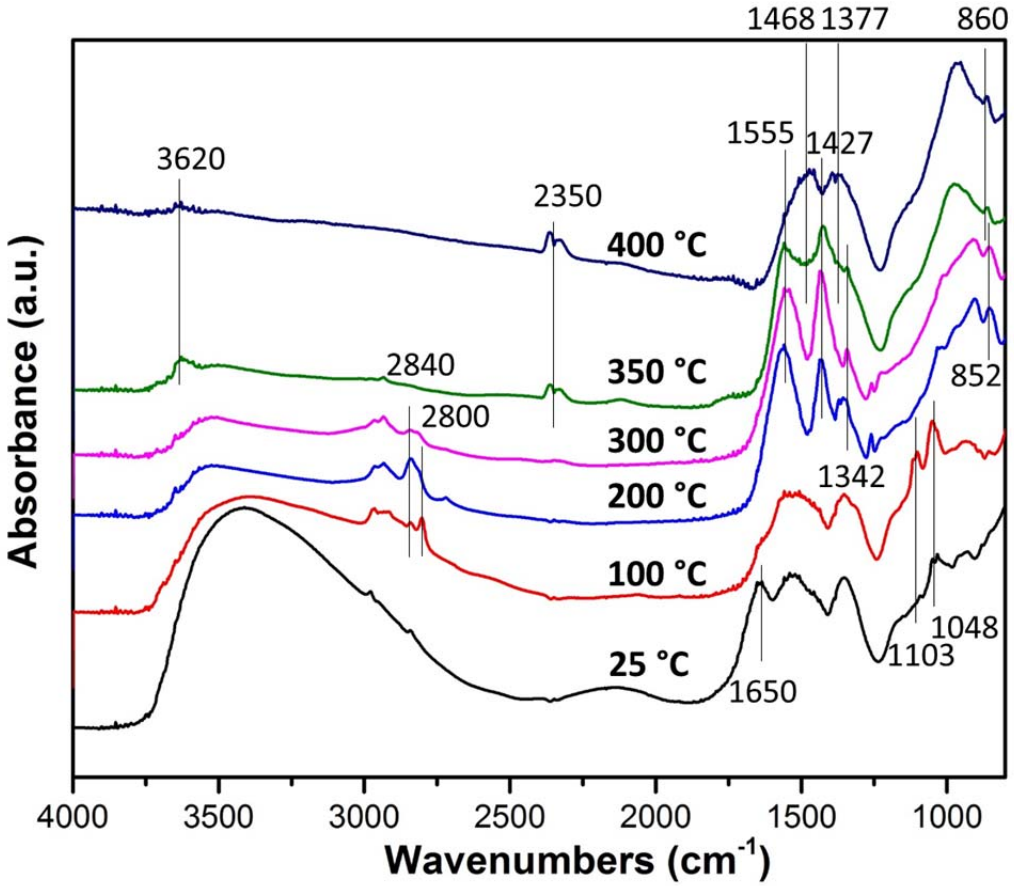

Figure 5 DRIFTS spectra for Ni/CeO_2 catalyst at elevating temperatures under methanol steam reforming conditions.

3.2. Methanol Reaction on Well-defined Ni-CeO_{2-x}(111) Model Surface

In our study of the Ni-CeO_2 powder catalysts above, we have identified the role of ceria as the active agent for water dissociation and we established that the generation of –OH groups is essential for the catalytic selectivity to CO_2 via the oxidation of surface species. However, further insights are still needed to reveal the actual surface process evolved with hydroxyl/methoxy species and to identify the interplay between the active metal and oxide support. Therefore, we shifted the study to a well-defined surface with careful control of Ni and CeOx surface features. The surface morphology of Ni/CeO_2(111) has been investigated by STM in a previous study [52]. Ni can be prepared as very small nanoparticles supported on CeO_2(111)

at 27 ^{o}C (700 K). Annealing to higher temperature induced some sintering of the Ni particles and large fraction of the Ni migrated into the ceria substrate to form a $Ce_{1-x}Ni_xO_{2-y}$ solid solution [20, 53].

The XPS data of Ce 4d + Ni 3p region from the as prepared Ni-CeO_{2-x}(111) surfaces are shown in Figure 6. The inset displays a close detail of the Ni 3p region. Fully oxidized ceria and reduced ceria could be distinguished in the Ce 4d by comparing the peak intensities at 122.8 eV and 126.1 eV, labeled as X′′′ and W′′′, respectively. These two features are solely associated with Ce^{4+} spin-orbit splitting [43]. Deconvolution of the Ce 4d spectrum indicates that the reduced film contained ~40% in Ce^{3+}, thus the surface is designated as Ni-$CeO_{1.8}$(111). As shown in the Ni 3p region, the results match well with previous studies [52-54]. During the annealing process of the sample preparation, most of the Ni was oxidized to Ni^{2+}, on the stoichiometric CeO_2 surface while significant amount of Ni remained metallic on the reduced ceria surface (CeO_{2-x}). Peak fitting of the Ni 3p region shown in the inset figure illustrates the ratio of two components. Integrating the peak area of each component points out that ~80 % and ~10% of the as-prepared Ni are present as metallic (Ni^0) on reduced and oxidized ceria, respectively.

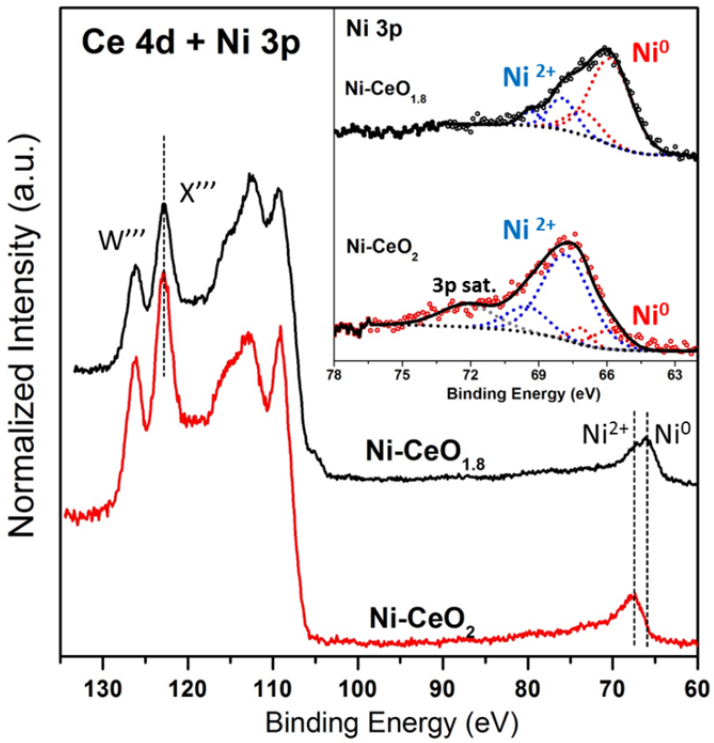

Figure 6 Ce 4d and Ni 3p of as-prepared surfaces, black line: Ni on reduced ceria film, red line: Ni on fully oxidized ceria film. Inset figure shows the peak deconvolution of Ni 3p region.

Regarding MSR chemistry, we first examined the methanol reaction on a Ni-CeO_2(111) surface. Figure 7 shows a series of XPS spectra collected for Ni-CeO_2(111) surface after 2L (Langmuir) dose of methanol at 27 ^oC (300 K) followed by sequentially heating up to 427 ^oC (700 K). In the O 1s region, at 27 ^oC (300 K), the lattice oxygen of ceria (530.4 eV) along with a shoulder at 532.5 eV could be identified. This peak (532.5 eV) can be attributed to the formation of methoxy and hydroxyls as a result of dissociative adsorption of methanol since, in the previous study of methanol on plain ceria [33], methanol is readily deprotonated on a ceria film at room temperature. Heating the surface up to 427 ^oC (700 K) leads to the vanishing of the peak, probably due to desorption of methanol. Similarly, in the C 1s region, a single peak (287.2 eV) corresponds to the methyl C as found in methoxy is seen at 27 ^oC (300 K). As the temperature increased to 227 ^oC (500 K), the peak intensity greatly decreases and shifts to higher binding energy at 287.9 eV. This indicates that either a new species is formed or the methoxy

adsorption configuration has changed. Upon heating up to 427 ^{o}C (700 K), all the carbon species has disappeared, leaving a carbon-free surface. The corresponding Ce 4d + Ni 3p XPS spectra was also recorded (not shown here). No reduction of Ni was detected due to the moderate dose of methanol (2L) and only a slight reduction of ceria (<5%) was seen. Based on this, and giving the fact that 90% of the Ni are 2+ as evidenced above, we can speculate that the fully oxidized Ni-CeO_2(111) surface is catalytically inert for methanol reaction, and only a small amount of methoxy formation is observed.

However, the behavior of methanol on the reduced Ni-$CeO_{1.8}$(111) surface is quite different, as shown in Figure 8a and b. In the O 1s spectra, a comparison with the signal in Figure 7 points to a significant enhancement in the relative intensity of hydroxyl/methoxy (-OH/CH_3O-) peaks, which is the result of the increased O vacancies on the reduced ceria for dissociative adsorption of methanol. The -OH/CH_3O- peak intensity again gradually attenuates and eventually disappears as the temperature increases to 427 ^{o}C (700 K). At 27 ^{o}C (300 K) of C 1s spectra (Figure 8b), the peak intensity of the methyl carbon located at 287.8 eV is higher than that of methyl carbon on the fully oxidized ceria surface. The shift to higher binding energy from oxidized to reduced ceria film has been observed before as methanol, ethanol and formaldehyde adsorption on plain ceria, due to the changes of surface work function upon surface reaction [33, 55, 56]. At 227 ^{o}C (500 K), the methoxy peak attenuates while a broad peak at 282-285 eV appears. This peak is assigned to a combination of C^0 (284.5 eV) and Ni carbide (Ni_3C) species (283.3 eV). Nickel carbide was similarly observed in the study of other hydrocarbon related molecules reacting with Ni [57-61]. The detection of Ni_3C here again enforces our earlier assignment of hex-Ni intermediate to Ni carbide phase in the XRD experiment. Besides the C^0/Ni_3C, a small amount of formate is also formed at 290.4 eV. Further heating the surface to

427 °C (700 K) causes the complete disappearance of the methoxy feature, leaving the surface only with C^0/Ni_3C because of the lack of an oxidative reactant. This result verifies that metallic Ni does activate methanol but is responsible for the undesired selectivity towards carbon.

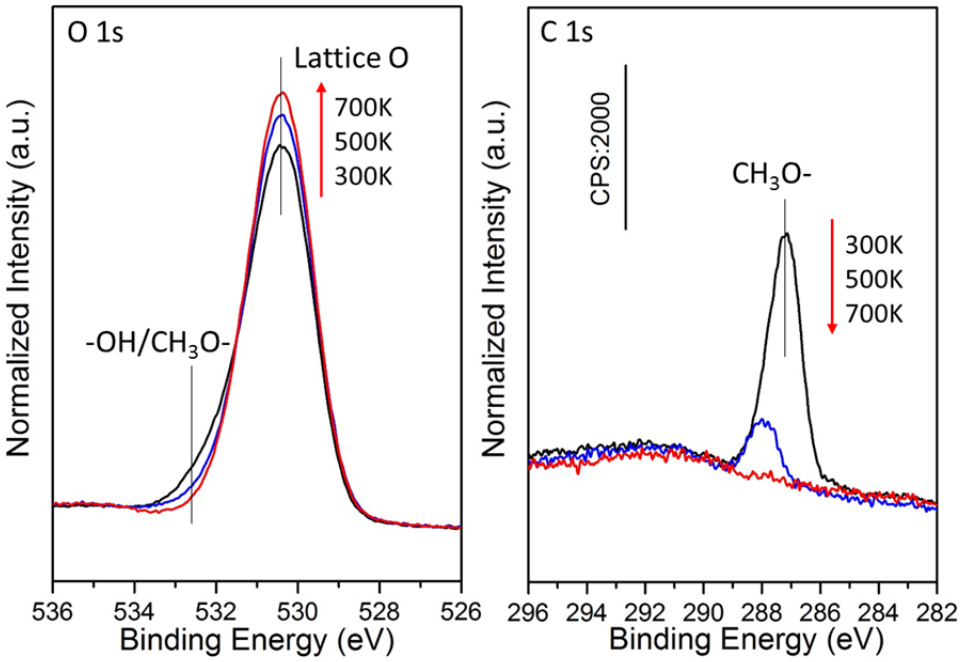

Figure 7 O 1s and C 1s of 2L methanol adsorption on Ni-CeO_2 surface at 27 °C (300 K) with subsequently heating up to 227 and 427 °C (500 and 700 K).

To check the effect of surface hydroxyl and water, another experiment was conducted by heating the pre-dosed methoxy covered surface in the background of 2×10^{-8} Torr of water, as shown in Figure 8c. Similarly, C^0/Ni_3C surface species formed at 227 °C (500 K) in the C 1s region. But upon increasing the temperature to 427 °C (700 K), a carbon-free surface is obtained, which highlights the role of hydroxyls/water on the selectivity of methanol steam reforming. Thus, by combining the *in situ* XRD/DRIFTS study of powder catalysts with a planar model system study, we can speculate that a possible reaction route for the MSR on Ni-CeO_2 catalyst occurs as follows:

On ceria site:

① $CH_3OH(g) \rightarrow CH_3O(a) + H(a)$, $CH_3O(a) + CeO_2 \rightarrow HCOO\text{-}(a) + 2H(a) + CeO_{2-x} + Vac$, or $CH_3O(a) + \text{-}OH(a) \rightarrow HCOO\text{-}(a) + 3H(a)$;

② $H_2O(g) + Vac \rightarrow Vac\text{-}OH(a) + H(a)$, $Vac\text{-}OH(a) \rightarrow O(lattice) + H(a)$;

③ $2H(a) \rightarrow H_2(g)$.

On Ni site or Ni-ceria interfaces:

④ $HCOO\text{-}(a) \rightarrow H(a) + CO_2(g)$,

or $HCOO\text{-} + O(lattice) \rightarrow CO_3^{2-} + H(a) \rightarrow CO_2(g) + O(lattice) + ½\ H_2(g)$;

However, a small amount of the methoxy may take an undesired pathway:

⑤ $CH_3O(a) \rightarrow CO(a) + 3H(a) \rightarrow C^0/Ni_3C + 3/2\ H_2(g)$;

⑥ $C^0/Ni_3C + 2O(lattice)/OH \rightarrow CO_2 + Ni^0 + H_2(g)$.

It is clear that both Ni and ceria contribute to the methanol steam reforming mechanism, and the metal-support interaction links the metal and oxide to complete the reaction cycle. Especially, it is the enhanced water dissociation on reduced ceria and then oxygen transfer from ceria to Ni that essentially enhances the surface oxidation ability of Ni, which in turn significantly improves the reaction selectivity at a higher temperature as we see in Figure 4.

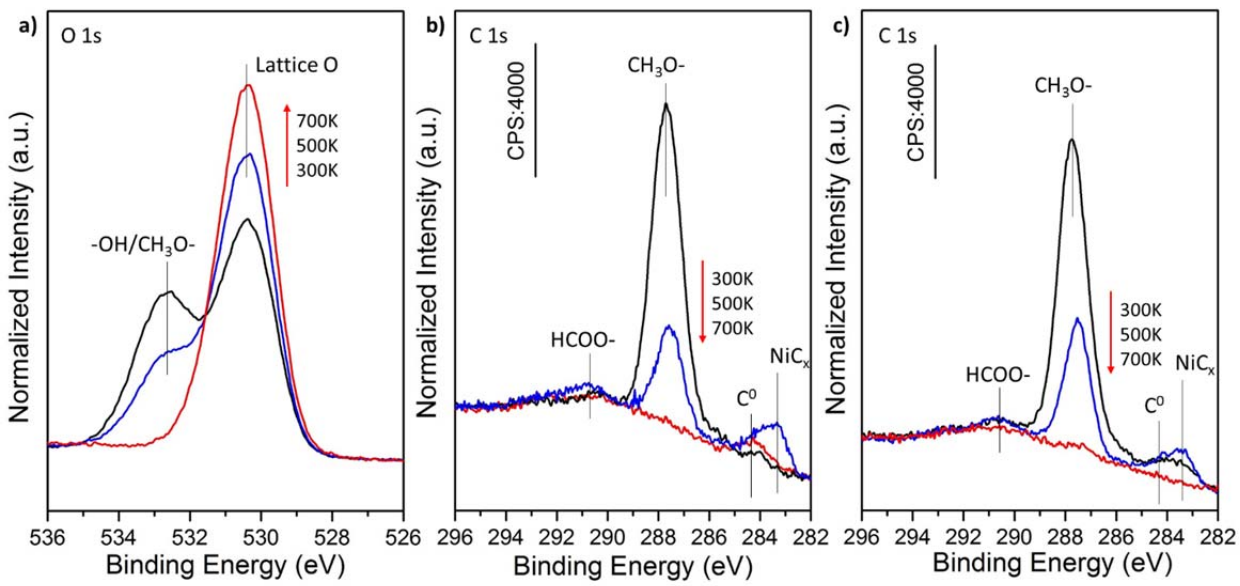

Figure 8 a) and b) O 1s and C 1s of 2L methanol adsorption on Ni-$CeO_{1.8}$(111) surface at 27 ^{o}C (300 K) with subsequently heating up to 227 and 427 ^{o}C (500 and 700 K); c) C 1s spectra of pre-dosed methanol surface at 300 K with subsequently heating up at a background of 2×10^{-8} Torr of water.

4. **Conclusion**

A comparative study between powder and model catalysts has been utilized to unravel the mechanism of the MSR reaction on nickel-ceria catalysts. *In situ* XRD and DRIFTS measurements were employed to study the phase transition and surface species of methanol steam reforming on a Ni-CeO_2 powder. Metallic Ni and partially reduced ceria were observed under steady-state reaction conditions. Post-reaction TEM of the samples showed carbon-free surfaces. The Ni-ceria catalyst exhibits a superior selectivity at a higher temperature when compared to a Cu catalyst prepared by the same method. The reaction intermediates identified from DRIFTS are methoxy, formate, carbonate and hydroxyl species. A modeling study of the methanol reaction on Ni-CeO_{2-x}(111) showed that the interplay of Ni and ceria through strong metal-support interactions is critical to the high selectivity for CO_2 production instead of surface carbon or CO formation.

Acknowledgement

The research carried out at Brookhaven National Laboratory, was supported by the U.S. Department of Energy, Office of Science and Office of Basic Energy Sciences under contract No. DE-SC0012704. This work used resources of the National Synchrotron Light Source (NSLS) and the Advanced Photon Source (20BM and 17BM) of Argonne National Laboratory (No. DE-AC02-06CH11357) which are DOE Office of Science User Facilities.

References

[1] A. Iulianelli, P. Ribeirinha, A. Mendes, A. Basile, Renew. Sustainable Energy Rev., 29 (2014) 355-368.
[2] S. Sá, H. Silva, L. Brandão, J.M. Sousa, A. Mendes, Appl. Catal. B, 99 (2010) 43-57.
[3] D.R. Palo, R.A. Dagle, J.D. Holladay, Chem. Rev., 107 (2007) 3992-4021.
[4] B.A. Peppley, J.C. Amphlett, L.M. Kearns, R.F. Mann, Appl. Catal. A, 179 (1999) 21-29.
[5] T. Shishido, Y. Yamamoto, H. Morioka, K. Takaki, K. Takehira, Appl. Catal. A, 263 (2004) 249-253.
[6] H. Jeong, K.I. Kim, T.H. Kim, C.H. Ko, H.C. Park, I.K. Song, J. Power Sources, 159 (2006) 1296-1299.
[7] J.K. Lee, J.B. Ko, D.H. Kim, Appl. Catal. A, 278 (2004) 25-35.
[8] H. Purnama, T. Ressler, R.E. Jentoft, H. Soerijanto, R. Schlögl, R. Schomäcker, Appl. Catal. A, 259 (2004) 83-94.
[9] Y.-H. Chin, R. Dagle, J. Hu, A.C. Dohnalkova, Y. Wang, Catal. Today, 77 (2002) 79-88.
[10] J. Rass-Hansen, C.H. Christensen, J. Sehested, S. Helveg, J.R. Rostrup-Nielsen, S. Dahl, Green Chemistry, 9 (2007) 1016-1021.
[11] K. Föttinger, J.A. van Bokhoven, M. Nachtegaal, G.n. Rupprechter, J. Phys. Chem. Lett., 2 (2011) 428-433.
[12] G. Jacobs, B.H. Davis, Appl. Catal. A, 285 (2005) 43-49.
[13] D.R. Ou, T. Mori, H. Togasaki, M. Takahashi, F. Ye, J. Drennan, Langmuir, 27 (2011) 3859-3866.
[14] C. Wang, M. Boucher, M. Yang, H. Saltsburg, M. Flytzani-Stephanopoulos, Appl. Catal. B, 154 (2014) 142-152.
[15] N. Yi, R. Si, H. Saltsburg, M. Flytzani-Stephanopoulos, Energy & Environmental Science, 3 (2010) 831-837.
[16] N. Iwasa, S. Masuda, N. Takezawa, React. Kinet. Catal. Lett., 55 (1995) 349-353.
[17] N. Laosiripojana, S. Assabumrungrat, J. Power Sources, 163 (2007) 943-951.
[18] J. Lu, X. Li, S. He, C. Han, G. Wan, Y. Lei, R. Chen, P. Liu, K. Chen, L. Zhang, Y. Luo, Int. J. Hydrogen Energy, 42 (2017) 3647-3657.
[19] W. Xu, Z. Liu, A.C. Johnston-Peck, S.D. Senanayake, G. Zhou, D. Stacchiola, E.A. Stach, J.A. Rodriguez, ACS Catalysis, 3 (2013) 975-984.
[20] Z. Liu, T. Duchoň, H. Wang, E.W. Peterson, Y. Zhou, S. Luo, J. Zhou, V. Matolín, D.J. Stacchiola, J.A. Rodriguez, S.D. Senanayake, J. Phys. Chem. C, 119 (2015) 18248-18256.
[21] J. Carrasco, D. López-Durán, Z. Liu, T. Duchoň, J. Evans, S.D. Senanayake, E.J. Crumlin, V. Matolín, J.A. Rodríguez, M.V. Ganduglia-Pirovano, Angew. Chem. Int. Ed., 54 (2015) 3917-3921.
[22] J. Carrasco, L. Barrio, P. Liu, J.A. Rodriguez, M.V. Ganduglia-Pirovano, J. Phys. Chem. C, 117 (2013) 8241-8250.
[23] A. Szizybalski, F. Girgsdies, A. Rabis, Y. Wang, M. Niederberger, T. Ressler, J. Catal., 233 (2005) 297-307.
[24] A. Haghofer, K. Föttinger, F. Girgsdies, D. Teschner, A. Knop-Gericke, R. Schlögl, G. Rupprechter, J. Catal., 286 (2012) 13-21.
[25] M.M. Günter, T. Ressler, R.E. Jentoft, B. Bems, J. Catal., 203 (2001) 133-149.
[26] E.S. Ranganathan, S.K. Bej, L.T. Thompson, Appl. Catal. A, 289 (2005) 153-162.
[27] J.N. Russell, S.M. Gates, J.T. Yates, Surf. Sci., 163 (1985) 516-540.
[28] J. Gong, D.W. Flaherty, R.A. Ojifinni, J.M. White, C.B. Mullins, J. Phys. Chem. C, 112 (2008) 5501-5509.
[29] J. Russell, I. Chorkendorff, J. Yates, Surf. Sci., 183 (1987) 316-330.

[30] S. Gates, J. Russell, J. Yates, Surf. Sci., 146 (1984) 199-210.
[31] J. Greeley, M. Mavrikakis, J. Am. Chem. Soc., 126 (2004) 3910-3919.
[32] D. Ehlers, A. Spitzer, H. Lüth, Surf. Sci., 160 (1985) 57-69.
[33] D.R. Mullins, M.D. Robbins, J. Zhou, Surf. Sci., 600 (2006) 1547-1558.
[34] A. Siokou, R.M. Nix, J. Phys. Chem. B, 103 (1999) 6984-6997.
[35] Z. Zhang, O. Bondarchuk, J. White, B.D. Kay, Z. Dohnálek, J. Am. Chem. Soc., 128 (2006) 4198-4199.
[36] K. Varazo, F. Parsons, S. Ma, D. Chen, J. Phys. Chem. B, 108 (2004) 18274-18283.
[37] V.r. Matolín, V. Johánek, M. Škoda, N. Tsud, K.C. Prince, T.s. Skála, I. Matolínová, Langmuir, 26 (2010) 13333-13341.
[38] W.Q. Xu, R. Si, S.D. Senanayake, J. Llorca, H. Idriss, D. Stacchiola, J.C. Hanson, J.A. Rodriguez, J. Catal., 291 (2012) 117-126.
[39] A.P. Hammersley, S.O. Svensson, M. Hanfland, A.N. Fitch, D. Hausermann, High Pressure Research, 14 (1996) 235-248.
[40] B.H. Toby, J. Appl. Crystallogr., 34 (2001) 210-213.
[41] A.C. Larson, R.B. Von Dreele, General Structure Analysis System. LANSCE, MS-H805, Los Alamos, New Mexico, (1994).
[42] N.S. Marinkovic, Q. Wang, A.I. Frenkel, J. Synchrotron Radiat., 18 (2011) 447-455.
[43] D. Mullins, S. Overbury, D. Huntley, Surf. Sci., 409 (1998) 307-319.
[44] D.R. Mullins, P.V. Radulovic, S.H. Overbury, Surf. Sci., 429 (1999) 186-198.
[45] F. Hoffmann, M. Weisel, C. Peden, Surf. Sci., 253 (1991) 59-71.
[46] M. Shishkin, T. Ziegler, J. Phys. Chem. C, 114 (2010) 21411-21416.
[47] G.N. Vayssilov, M. Mihaylov, P.S. Petkov, K.I. Hadjiivanov, K.M. Neyman, J. Phys. Chem. C, 115 (2011) 23435-23454.
[48] G. Jacobs, L. Williams, U. Graham, G.A. Thomas, D.E. Sparks, B.H. Davis, Appl. Catal. A, 252 (2003) 107-118.
[49] C. Binet, M. Daturi, J.-C. Lavalley, Catal. Today, 50 (1999) 207-225.
[50] D. Gamarra, A. Martínez-Arias, J. Catal., 263 (2009) 189-195.
[51] A. Goguet, F.C. Meunier, D. Tibiletti, J.P. Breen, R. Burch, J. Phys. Chem. B, 108 (2004) 20240-20246.
[52] Y. Zhou, J.M. Perket, A.B. Crooks, J. Zhou, J. Phys. Chem. Lett., 1 (2010) 1447-1453.
[53] S.D. Senanayake, J. Evans, S. Agnoli, L. Barrio, T.-L. Chen, J. Hrbek, J.A. Rodriguez, Top. Catal., 54 (2011) 34-41.
[54] Y. Zhou, J. Zhou, J. Phys. Chem. C, 116 (2012) 9544-9549.
[55] J. Zhou, D.R. Mullins, Surf. Sci., 600 (2006) 1540-1546.
[56] D.R. Mullins, S.D. Senanayake, T.L. Chen, J. Phys. Chem. C, 114 (2010) 17112-17119.
[57] M. Sarr, N. Bahlawane, D. Arl, M. Dossot, E. McRae, D. Lenoble, J. Phys. Chem. C, 118 (2014) 23385-23392.
[58] I. Czekaj, F. Loviat, F. Raimondi, J. Wambach, S. Biollaz, A. Wokaun, Appl. Catal. A, 329 (2007) 68-78.
[59] C. Ducati, I. Alexandrou, M. Chhowalla, J. Robertson, G.A.J. Amaratunga, J. Appl. Phys., 95 (2004) 6387-6391.
[60] C. Klink, I. Stensgaard, F. Besenbacher, E. Lægsgaard, Surf. Sci., 342 (1995) 250-260.
[61] R.S. Weatherup, L. D'Arsié, A. Cabrero-Vilatela, S. Caneva, R. Blume, J. Robertson, R. Schloegl, S. Hofmann, J. Am. Chem. Soc., 137 (2015) 14358-14366.